A Novel Dual-Axis Repulsive Maglev Guiding System With Permanent Magnet: Modeling and Controller Design

Mei-Yung Chen, *Student Member, IEEE*, Ming-Jyh Wang, and Li-Chen Fu, *Senior Member, IEEE*

***Abstract*—In this paper, we extend our previous result on designing a single-axis Maglev guiding system to a more involved task of designing a novel dual-axis positioning system. First of all, important issues related to construction of the mechanism of the dual-axis positioning system are addressed. Then, the dynamics of the dual-axis Maglev guiding system are analyzed. According to the derived analytic model, which is subject to unknown system parameters, an adaptive controller that can control the carrier at the desired target point of each axis with full alignment is presented. From the experiment results, a good performance in terms of regulation of the guiding-axis and tracking of the positioning-axis is achieved. This validates the design of the system hardware and demonstrates the feasibility of the developed controller.**

***Index Terms*—Adaptive control, dual-axis Maglev, hybrid magnet, precision guiding.**

I. Introduction

DUE TO THE noncontact property of magnetic levitation technology, a resulting system possesses many advantages, such as no friction, no contamination, long life, high speed, low noise and so on. According to Hollis *et al.* [1], the system creates a stable state without any mechanical contact when the gravitational force is solely counterbalanced by magnetic forces. Prior work on Maglev systems has spanned many fields. A large volume of literature has been published. This subject has attracted much interest in the areas of transportation [2], [3], magnetic bearings [4], [5], high-resolution positioning systems [6], [7], vibration-isolation tables [8], wind tunnels [9] and so on. Furthermore, as industrial technologies have continuously advanced, high-precision positioning has come to play a more and more important role in a variety of high-tech areas, such as integrated-circuit photolithography [10] (stepper and repeat positioning), material science (tunneling microscopy), medicine and biology (cell biology research). Some of these technologies must be employed in a high-quality clean room or in a vacuum environment. In order to meet this requirement, more stringent manufacturing processes and advanced fabrication equipment must be developed. Here, however, we will only investigate the Maglev techniques related to the field of larger (centimeter level) moving range with precision guidance, and we will report on our design and implementation of a prototype Maglev system, which was carried out to verify its high precision performance.

The Maglev control problem is complicated due to the inherent nonlinearities associated with the electro-mechanical dynamics. Besides these nonlinearities, the controller design has to compensate for some modeling error which cause natural vibration in the system. Therefore, the controller to be developed should be robust enough to tolerate these system uncertainties and unmodeling dynamics. Many conventional controllers for Maglev systems are based on the proportional-integral-differential strategy [11], or the pole-placement control method [12]. This paper focused on adaptive control because it is robust to parameter uncertainties and disturbances [17], [18].

In our previous research [13]–[16], we analyzed the dynamics of a single-axis Maglev guiding system and derived its analytical model, and we proposed an adaptive controller which deals with unknown parameters to regulate the system attitude. Based on the above-mentioned works on a single-axis guiding system, we developed a novel dual-axis Maglev guiding system in this study. It is a repulsive Maglev system consisting of two single-axis guiding subsystems. The guiding system, including sensors and drivers, was implemented. Experimental results are provided here to demonstrate the feasibility of this proposed design for a dual-axis Maglev guiding system. Furthermore, a satisfactory performance in terms of stiffness and high resolution was achieved.

The organization of this paper is as follows. Section II describes the design aspects of the prototype system proposed here, and provides a detailed mathematic model. In Section III, an adaptive controller for the prototype Maglev system is presented, which can achieve the regulating objective for guidance and the tracking objective for positioning. Section IV presents extensive experimental results to demonstrate the effectiveness of the system design, including the adaptive controller. Some discussions are also given in Section IV. Finally, conclusions are drawn in Section V.

Manuscript received August 15, 2001; revised May11, 2002. Recommended by Technical Editor D. Mavroidis. This work was sponsored by the National Science Council, R.O.C., under Grant NSC 87-2213-E-002-092.

M.-Y. Chen is with the R242, Department of Electrical Engineering, National Taiwan University, Taipei 106, Taiwan, R.O.C. (e-mail:cmy@cc.ee.ntu.edu.tw).

M.-J. Wang is with the Chung-Shan Institute of Science and Technology, Chung-Li, Taiwan, R.O.C.

L.-C. Fu is with the R524, Department of Electrical Engineering, National Taiwan University, Taipei, Taiwan, R.O.C. and also with the R533, Department of Computer Science and Information Engineering, National Taiwan University, Taipei, Taiwan, R.O.C. (e-mail:lichen@ccms.ntu.edu.tw).

Digital Object Identifier 10.1109/TMECH.2003.809158

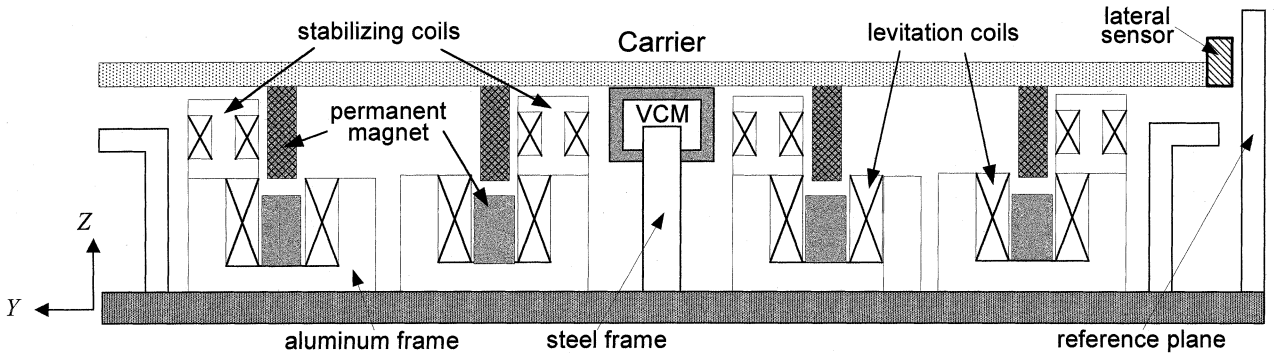

Fig. 1. Front view of Subsystems I and II.

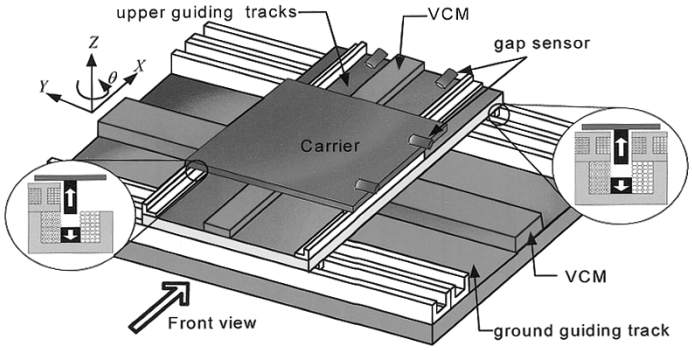

Fig. 2. 3-D view of the dual-axis Maglev positioning system.

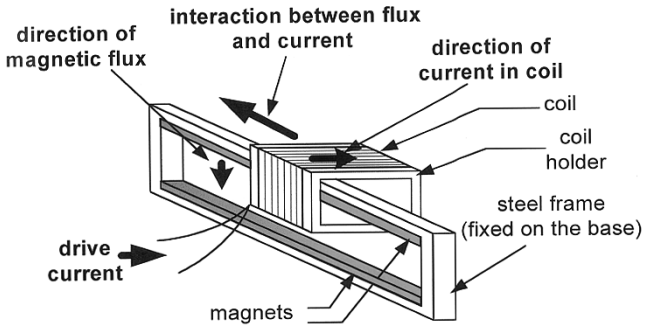

Fig. 3. Perspective of the VCM and track.

II. System Description and Modeling

In this section, the mechanical structure of a Maglev guiding system will be described. Its analytical model will be derived and analyzed.

A. Maglev Guiding System

In a stepper, one often adopts a linear slide which supports and guides the carrier. The system proposed here is featured by an active control which provides a contactless linear slide but is different from the magnetic bearing of a rotating machine. In our earlier work, a restricted version with one axis was proposed and then used as the basis for the present two-axis design. For design details of that system, the reader can refer to [14]. In the context described below, only a brief review of the design is given.

The features of this two-axis Maglev guiding system include: 1) repulsive levitation; 2) hybrid magnets; 3) a passive carrier and active track; 4) an oblong coil; and 5) a four-track design. Subsystem I includes a carrier, permanent magnets and a modified voice-coil motor (VCM), and Subsystem II includes upper guiding tracks, permanent magnets and a VCM, respectively. Referring to Fig. 1, which shows Subsystems I and II, the permanent magnets and the winding coils inside each track together are called the levitator, and the winding coils along the sides of the tracks are called the stabilizer. A three-dimensional (3-D) view of the dual-axis Maglev system is shown in Fig. 2. Subsystem I moves along Subsystem II in the X direction, whereas Subsystem II moves along the ground guiding tracks in the Y direction. The ground guiding system must levitate Subsystem II, which levitates Subsystem I.

To facilitate the design task, one must reduce the combined weight of Subsystems I and II as much as possible. Also, reducing the weight of Subsystem I helps to reduce the dynamic coupling between the two Subsystems while Subsystem I is moving along Subsystem II. Then, once the weight of Subsystem II is reduced, excessive coil currents or coil turns that lead to a significant magnetic field can be avoided, which in turn alleviates undesirable disturbance to the system. To achieve such weight reduction, the approach adopted here places light permanent magnets inside the tracks instead of using a large number of coil turns to reduce the total weight. A side benefit of adding permanent magnets is that power consumption is reduced since the major counter-gravitational force is attributable to the permanent magnets. Another way of achieving weight reduction is to reduce the length of the upper guiding tracks due to the fact that each levitation magnet beneath Subsystem I never traverses the full length of the track, so that the length of each retaining track is apparently shorter than that of the upper guiding tracks as shown in Fig. 2.

B. Modified VCM

To provide propulsion force in the Y direction, we adopt a modified VCM as shown in Fig. 3. Its most salient feature is its lack of contact. The design of the modified VCM is similar to that of a linear motor with exception that it (the modified VCM) does not have stepwise nature. Therefore, the actuation resolution reaches the limit of the digital signal acquisition device.

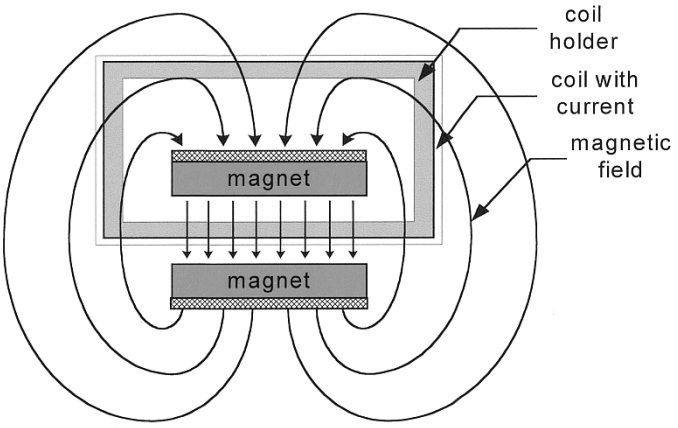

Fig. 4. Magnetic field from two permanent magnets.

The propulsion force of the VCM results from the interaction between the magnetic field generated by the permanent magnet and the coil. The magnetic field created by the permanent magnets is shown in Fig. 4. The working principle of the VCM is to generate a pushing force F along the track, as given by

$$F = i\vec{L} \times \vec{B} \tag{1}$$

where i is the input current, L is the length of the flux path and B is the flux distribution in the free space. In practice, the direction of current is perpendicular to the direction of the flux in the mechanism, so that we derive the value of the interaction force as

$$F = iLB. \tag{2}$$

The force in this design is more powerful than that in the traditional VCM, where the moving coil encloses one edge of the rectangular steel frame, on which two bar magnets are attached parallel to its inner side as the magnetic core. The whole mechanism functions as a rail. The reasons for this design are as follows. Because both edges are associated with magnet bars as shown in Fig. 4, the VCM has higher magnetic intensity since an air gap between two edges will exhibit higher magnetic flux density. Also, because of the arrangement of the two magnetic edges facing each other, the interior magnetic field tends to be perpendicular to the coil across the air gap; that is, the magnetic field can be more effective. As a result, motion control can be accomplished more easily using less control current in the coil.

C. Simplified Model of the Dual-Axis Maglev System

In the structure mentioned above, there obviously exists coupling between Subsystem I and II, and we cannot control them independently. Here, we will present a dual-axis model, including the dynamics of Subsystem I and II, but we will concentrate on the unstable modes. For later reference, we will refer to this mechanism as a dual-axis model for two floating bodies.

Before modeling, several assumptions must be made here in order to simplify the modeling process, namely:

- the repulsive levitation design yields two floating bodies which are laterally unstable but vertically stable, where the unstable modes can be decoupled from the stable ones [12];
- the magnetic forces and torques between the levitation magnets and stabilizing coils can be linearized about the small displacements in the x direction and small rotations in the θ direction;
- the stiffness of the ground guiding tracks in the vertical direction is strong enough (or the weight of Subsystem I is light enough) so that the disturbances induced by the moving range of the floating body can be neglected.

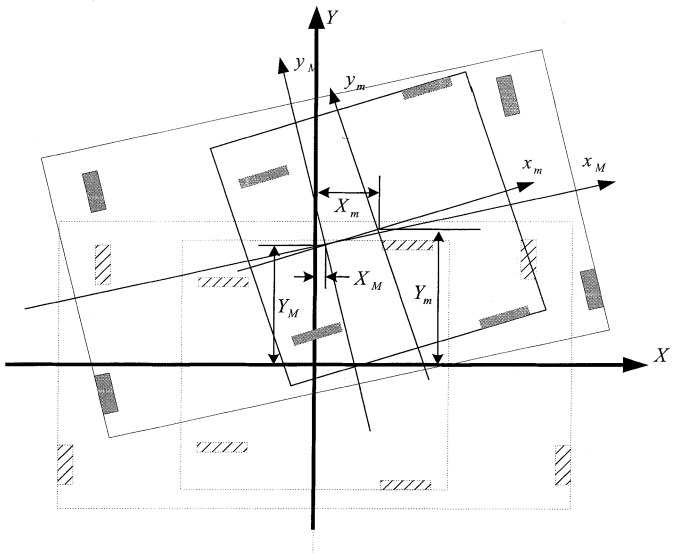

Fig. 5. Relative motions of the Maglev system.

Now considering only the lateral direction, we can observe that each levitation magnet beneath the carrier is subject to a destabilizing force F_d from the levitator if the levitation magnet is not at the center of the track, and a stabilizing force F_s from the stabilizer to the center of the track as shown in Figs. 7 and 8. We can rewrite them in a more general form as [12]

$$F_d = K_d s \tag{3}$$

$$F_s = -K_i I_s \tag{4}$$

where K_d is a positive value, called a destabilization force constant here, K_i is a positive constant related to the stabilizing force, s is the displacement, and I_s is the control current in the stabilizer. If the vertical direction disturbance from the VCM is negligible (assuming it is much smaller than the high stiffness produced by the levitator), the propulsion force can be simplified as

$$F_c = K_c I_c \tag{5}$$

where K_c is a positive constant for the VCM and I_c is the control current in the VCM.

Here, XYZ denotes the global coordinate system with Z pointing out of paper. The local coordinates $\{x_m y_m z_m\}$, $\{x_M y_M z_M\}$ are chosen to be coincident with Subsystem I and II's principal axes, respectively, so that the products of inertia can be zero as shown in Fig. 5. We denote that Subsystems I and II undergo displacements X_m, Y_m, θ_m and X_M, Y_M, θ_M, respectively, where X_m is Subsystem I's long-range movements

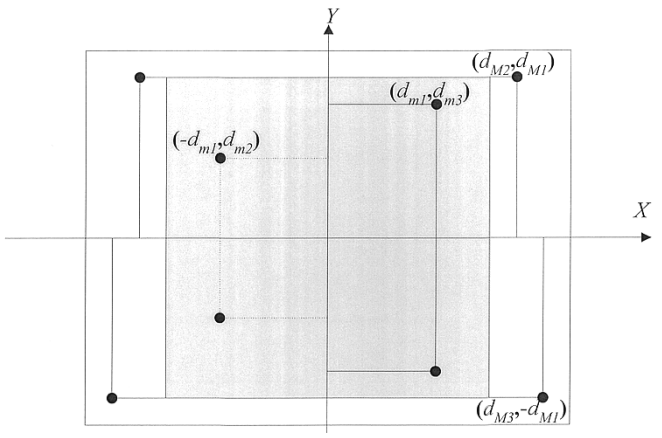

Fig. 6. Positions of the levitation magnets in the dual-axis Maglev system.

and Y_M is Subsystem II's long-range movements, respectively. For simplicity, we further assume that the forces applied to the levitation magnets beneath the carrier board are concentrated on their central point.

To obtain the equations of motion for a rigid body, we have

$$\sum F = m\ddot{X} \tag{6}$$

$$\sum T = J\ddot{\theta} \tag{7}$$

where F and T denote the external force and torque, respectively, whereas m and J denote the mass and inertia with respect to the z axis of the rigid body, respectively.

Now, we can derive the equations of motion for Subsystem II. The positions of the levitation magnets are shown as Fig. 6, and the relative displacements of the Subsystem II magnets in ground coordinates are

$$\begin{bmatrix} D_X(a,b) \\ D_Y(a,b) \end{bmatrix} = \begin{bmatrix} X_M \\ Y_M \end{bmatrix} + U(-\theta_M)\begin{bmatrix} a \\ b \end{bmatrix} \tag{8}$$

where $U(\theta) \equiv \begin{bmatrix} \cos\theta & \sin\theta \\ -\sin\theta & \cos\theta \end{bmatrix}$ is the transformation matrix and (a,b) represents the positions of the levitation magnets mounted on the upper guiding tracks.

Forces exerted by the ground guiding tracks on Subsystem II from (3) to (5) are

$$\begin{aligned} X \text{ direction}: & \begin{cases} F_{\mathrm{Msi}} = -K_{\mathrm{Ms}} I_{\mathrm{Mi}} \quad \text{(inner pair)} \\ F_{\mathrm{Mso}} = -K_{\mathrm{Ms}} I_{\mathrm{Mo}} \quad \text{(outer pair)} \\ F_{\mathrm{Mdi}} = K_{\mathrm{Md}} D_X(-d_{M2}, d_{M1}), \\ F_{\mathrm{Mdo}} = K_{\mathrm{Md}} D_X(-d_{M3}, -d_{M1}) \end{cases} \\ Y \text{ direction}: & \quad F_{\mathrm{Mc}} = K_{\mathrm{Mc}} I_{\mathrm{Mc}} \end{aligned} \tag{9}$$

where F_{Msi}, F_{Mso} are stabilizing forces caused by the inner pair of stabilizers and the outer pair of stabilizers in the ground guiding tracks, respectively; F_{Mdi} and F_{Mdo} are destabilizing forces caused by the inner levitator and the outer levitator in the ground guiding tracks, respectively, as shown in Fig. 7; F_{Mc} is exerted by the VCM in Subsystem II; I_{Mi}, I_{Mo}, and I_{Mc} are control currents in the inner stabilizer, the outer stabilizer and the VCM, respectively. After substitution of (9) into (6) and (7), the motion equations of Subsystem II can be obtained as

$$\begin{aligned} M\ddot{X}_M =& 2(F_{\mathrm{Msi}} + F_{\mathrm{Mso}} + F_{\mathrm{Mdi}} + F_{\mathrm{Mdo}}) \\ & + 2(F_{\mathrm{msi}} + F_{\mathrm{mso}} + F_{\mathrm{mdi}} + F_{\mathrm{mdo}}) \\ & \sin\theta_M - F_{\mathrm{mc}} \cos\theta_M \\ M\ddot{Y}_M =& K_{\mathrm{MC}} I_{\mathrm{MC}} - 2(F_{\mathrm{msi}} + F_{\mathrm{mso}} + F_{\mathrm{mdi}} + F_{\mathrm{mdo}}) \\ & \cos\theta_M - F_{\mathrm{mc}} \sin\theta_M \\ J_M\ddot{\theta}_M =& 2(F_{\mathrm{Mso}} + F_{\mathrm{Mdo}}) d_{M1} \cos\theta_M \\ & - 2(F_{\mathrm{Msi}} + F_{\mathrm{Mdi}}) d_{M1} \cos\theta_M \\ & - 2(F_{\mathrm{mso}} + F_{\mathrm{mdo}}) l_{\mathrm{ox}} - 2(F_{\mathrm{msi}} + F_{\mathrm{mdi}}) l_{\mathrm{ix}} \end{aligned}$$

where

$$\begin{aligned} \begin{bmatrix} l_{ox} \\ l_{\mathrm{oy}} \end{bmatrix} =& U(\theta_M)\left(\begin{bmatrix} X_m \\ Y_m \end{bmatrix} + U(-\theta_m)\begin{bmatrix} d_{m1} \\ -d_{m3} \end{bmatrix} - \begin{bmatrix} X_M \\ Y_M \end{bmatrix}\right) \\ \begin{bmatrix} l_{\mathrm{ix}} \\ l_{\mathrm{iy}} \end{bmatrix} =& U(\theta_M)\left(\begin{bmatrix} X_m \\ Y_m \end{bmatrix} + U(-\theta_m)\begin{bmatrix} -d_{m1} \\ -d_{m2} \end{bmatrix} - \begin{bmatrix} X_M \\ Y_M \end{bmatrix}\right) \end{aligned} \tag{10}$$

and M, J_M are the mass and moment of inertia of Subsystem II, respectively. The term $[l_{\mathrm{ox}}, l_{\mathrm{oy}}]^T$ is the displacement of an outer track levitation magnet mounted on the carrier in the $\{x_M y_M z_M\}$ coordinate system, whereas the term $[l_{\mathrm{ix}}, l_{\mathrm{iy}}]^T$ is that of an inner track one.

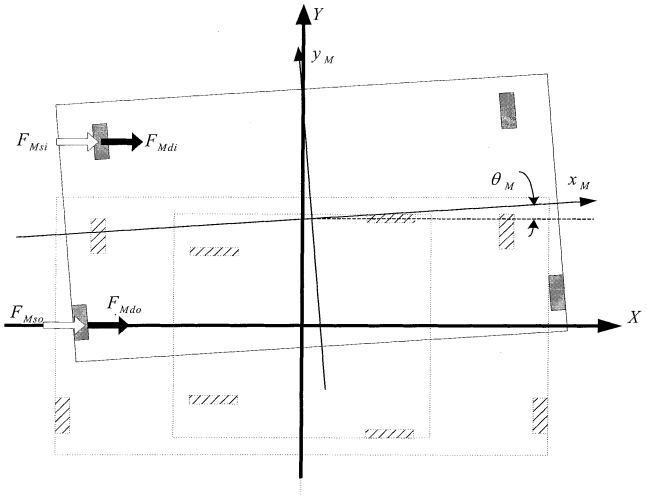

Fig. 7. Subsystem II of the dual-axis Maglev system.

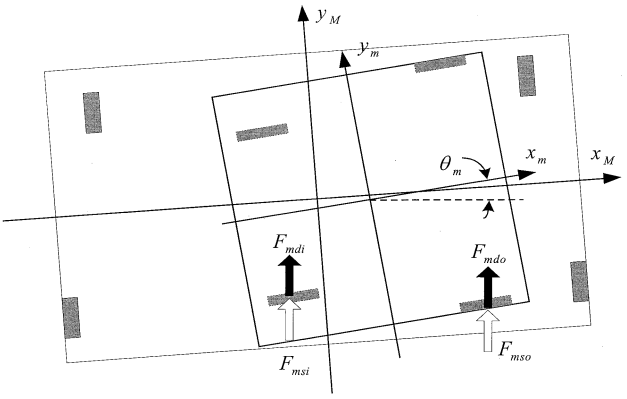

Fig. 8. Subsystem I of the dual-axis Maglev system.

Then, we derive the equations of motion for Subsystem I. The relative displacements of the levitation magnets between Subsystem I and II on the $\{x_M y_M z_M\}$ coordinate system can be obtained as

$$\begin{bmatrix} D_x(c,d) \\ D_y(c,d) \end{bmatrix} = U(\theta_M)\left\{\left(\begin{bmatrix} X_m \\ Y_m \end{bmatrix} + U(-\theta_M)\begin{bmatrix} c \\ d \end{bmatrix}\right) - \left(\begin{bmatrix} X_M \\ Y_M \end{bmatrix} + U(-\theta_M)\begin{bmatrix} c \\ d \end{bmatrix}\right)\right\} \quad (11)$$

where (c,d) represents the positions of levitation magnets mounted on the carrier.

We have grouped the stabilizers into an inner pair and an outer pair, and similarly, for the levitators. Forces from Subsystem II to Subsystem I from (3)to (5) are

$$\begin{aligned} Y \text{ direction}: & \begin{cases} F_{\mathrm{msi}} = -K_{\mathrm{ms}} I_{\mathrm{mi}} \quad \text{(inner pair)} \\ F_{\mathrm{mso}} = -K_{\mathrm{ms}} I_{\mathrm{mo}} \quad \text{(outer pair)} \\ F_{\mathrm{mdi}} = K_{\mathrm{md}} D_y(-d_{m1}, d_{m2}) \\ F_{\mathrm{mdo}} = K_{\mathrm{md}} D_y(-d_{m1}, -d_{m3}) \end{cases} \\ X \text{ direction}: & \quad F\mathrm{mc} = K_{\mathrm{mc}} I_{\mathrm{mc}} \end{aligned} \quad (12)$$

where F_{msi}, F_{mso} are stabilizing forces caused by the inner pair of stabilizers and the outer pair of stabilizers in Subsystem II, respectively; F_{mdi} and F_{mdo} are destabilizing forces caused by the inner levitators and the outer levitators in Subsystem II, respectively as shown in Fig. 8; F_{mc} is exerted by the VCM in Subsystem II; I_{mi}, I_{mo}, and I_{mc} are control currents in the inner stabilizer, the outer stabilizer and the VCM, respectively. The motion equations of Subsystem I after substitution of (12) into (6) and (7) become

$$\begin{aligned} m\ddot{Y}_m =& 2(F_{\mathrm{msi}} + F_{\mathrm{mso}} + F_{\mathrm{mdi}} + F_{\mathrm{mdo}})\cos\theta_M \\ &+ F_{\mathrm{mc}} \sin\theta_M \\ m\ddot{X}_m =& -2(F_{\mathrm{msi}} + F_{\mathrm{mso}} + F_{\mathrm{mdi}} + F_{\mathrm{mdo}})\sin\theta_M \\ &+ F_{\mathrm{mc}} \cos\theta_M \\ J_m\ddot{\theta}_m =& 2(F_{\mathrm{mso}} + F_{\mathrm{mdo}})d_{m1}\cos(\theta_m - \theta_M) \\ &- 2(F_{msi} + F_{\mathrm{mdi}})d_{m1}\cos(\theta_m - \theta_M) \end{aligned} \quad (13)$$

where m, J_m are the mass and moment of inertia of Subsystem I, respectively.

Observing the mechanical design, we can assume that $Y_m - Y_M$, X_M, θ_m, and θ_M are small displacements so that the higher order terms are set to zero and $\sin\theta_m \cong \theta_m$ $\cos\theta_m \cong 1$, $\sin\theta_M \cong \theta_M$ and $\cos\theta_M \cong 1$. After substituting and simplifying the equations of motion of the whole system, we can obtain the following dynamic model in (14), shown at the bottom of page.

III. Controller Design of the Dual-Axis Positioning System

Based on the modeling process described in the previous section, several assumptions have been made, which inevitably will cause some modeling errors. Therefore, the controller to be developed should be robust enough to tolerate these system uncertainties and unmodeling dynamics.

Based on our experimental experience, we will design an adaptive control for the Maglev system, which can on-line perform system identification implicitly or explicitly while tuning the controller gains so as to guarantee the stability of the closed-loop system, especially in the case of a definite model structure with unknown parameters and variable loads. Nowadays, high-speed PC-based controllers are becoming more and more economical and reliable when it comes to intensive computations performed to realize a complex adaptive control scheme. This fact, therefore, motivates us to adopt an adaptive controller.

A. Plant Model

For stability analysis, we assign the control input, states and unknown force constants as follows:

$$\begin{aligned} \mathbf{u} &= [u_1\ u_2\ u_3\ u_4\ u_5\ u_6]^T \\ &= [I_{\mathrm{mc}}\ I_{\mathrm{mi}} + I_{\mathrm{mo}}\ I_{\mathrm{mo}} - I_{\mathrm{mi}}\ I_{\mathrm{Mi}} \\ &\quad + I_{\mathrm{Mo}}\ I_{\mathrm{Mc}}\ I_{\mathrm{Mo}}\ - I_{\mathrm{Mi}}]^T \\ \mathbf{x} &= [x_1\ x_2\ x_3\ x_4\ x_5\ x_6]^T \end{aligned} \quad (15)$$

$$\begin{bmatrix} m\ddot{X}_m \\ m\ddot{Y}_m \\ J_m\ddot{\theta}_m \\ M\ddot{X}_M \\ M\ddot{Y}_M \\ J_M\ddot{\theta}_M \end{bmatrix} = \begin{bmatrix} 0 \\ 4K_{\mathrm{md}}(Y_m - Y_M) - 4K_{\mathrm{md}}X_m\theta_M \\ 4K_{\mathrm{md}}d_{m1}^2(\theta_m - \theta_M) \\ 4K_{\mathrm{Md}}X_M \\ -4K_{\mathrm{md}}(Y_m - Y_M) + 4K_{\mathrm{md}}X_m\theta_M \\ 4K_{\mathrm{Md}}d_{M1}^2\theta_M - 4K_{\mathrm{md}}(Y_m - Y_M - X_m\theta_m)X_m - 4K_{\mathrm{md}}d_{m1}^2(\theta_m - \theta_M) \end{bmatrix} + \begin{bmatrix} 2K_{\mathrm{ms}}(I_{\mathrm{mi}} + I_{\mathrm{mo}})\theta_M + K_{\mathrm{mc}}I_{\mathrm{mc}} \\ -2K_{\mathrm{ms}}(I_{\mathrm{mi}} + I_{\mathrm{mo}}) + K_{\mathrm{mc}}I_{\mathrm{mc}}\theta_M \\ -2K_{\mathrm{ms}}(I_{\mathrm{mo}} + I_{\mathrm{mi}})d_{m1} \\ -2K_{\mathrm{Ms}}(I_{\mathrm{Mi}} + I_{\mathrm{Mo}}) - 2K_{\mathrm{ms}}(I_{\mathrm{mi}} + I_{\mathrm{mo}})\theta_M - K_{\mathrm{mc}}I_{\mathrm{mc}} \\ K_{\mathrm{Mc}}I_{\mathrm{Mc}} + 2K_{\mathrm{ms}}(I_{\mathrm{mi}} + I_{\mathrm{mo}}) - K_{\mathrm{mc}}I_{\mathrm{mc}}\theta_M \\ T_{M1} + T_{M2} \end{bmatrix}$$

$$T_{M1} = 2K_{\mathrm{Ms}}(I_{\mathrm{Mo}} - I_{\mathrm{Mi}})d_{M1} + 2K_{\mathrm{ms}}(X_m - X_M)(I_{\mathrm{mi}} + I_{\mathrm{mo}})$$

where

$$T_{M2} = 2K_{\mathrm{ms}}d_{m1}(I_{\mathrm{mo}} - I_{\mathrm{mi}}) + 2K_{\mathrm{ms}}(\theta_m - \theta_M)(d_{m2}I_{\mathrm{mi}} + d_{m3}I_{\mathrm{mo}}) \quad (14)$$

$$= [X_m\ Y_m - Y_M\ \theta_m\ X_M\ Y_M\ \theta_M]^T \quad (16)$$

$$\mathbf{K} = [K_{\rm ms}\ K_{\rm md}\ K_{\rm mc}\ K_{\rm Ms}\ K_{\rm Md}\ K_{\rm Mc}]^T = [K_1\ K_2\ K_3\ K_4\ K_5\ K_6]^T. \quad (17)$$

Now, the model in (14) can be transformed into

$$\mathbf{D}\ddot{\mathbf{x}} = \mathbf{f}(\mathbf{x}, \mathbf{K}) + \mathbf{B}(\mathbf{x}, \mathbf{K})\mathbf{u} \quad (18)$$

where

$$\mathbf{D} = \text{diag}\frac{m, Mm}{M+m}, J_m, M, M, J_M > 0$$

$$\mathbf{f}(\mathbf{x}, \mathbf{K}) = \begin{bmatrix} 0 \\ 4K_2x_2 - 4K_2x_1x_6 \\ 4K_2d_{m1}^2(x_3 - x_6) \\ 4K_5x_4 \\ -4K_2x_2 + 4K_2x_1X_6 \\ 4K_5d_{M1}^2x_6 - 4K_2(x_2 - x_1x_3)x_1 - 4K_2d_{m1}^2(x_3 - x_6) \end{bmatrix},$$

$$\mathbf{B}(\mathbf{x}, \mathbf{K}) = \begin{bmatrix} K_3 & 2K_1x_6 & 0 & 0 & 0 & 0 \\ K_3x_6 & -2K_1 & 0 & 0 & \frac{m}{M+m}K_6 & 0 \\ 0 & 0 & 2K_1d_{m1} & 0 & 0 & 0 \\ -K_3 & 2K_1x_6 & 0 & -2K_4 & 0 & 0 \\ K_3x_6 & 2K_1 & 0 & 0 & K_6 & 0 \\ 0 & K_{T1} & K_{T2} & 0 & 0 & -2K_4d_{M1} \end{bmatrix}.$$

Also, the terms K_{T1} and K_{T2} in $\mathbf{B}(\mathbf{x}, \mathbf{K})$ are

$$K_{T1} = 2K_1(x_1 - x_4) + K_1(d_{m2} + d_{m3})(x_3 - x_6)$$
$$K_{T2} = 2K_1d_{m1} + K_1(d_{m3} - d_{m2})(x_3 - x_6).$$

Based on the definition in (16), we can describe the control objective as follows: *Let x_2, x_3, x_4, and x_6 approach zero, and let x_1 and x_5 approach x_d and y_d, respectively, which implies that the carrier will go to the desired position (x_d,y_d) and maintain Subsystems I and II at the center of the upper guiding tracks and ground guiding tracks, respectively*.

Before deriving the control and adaptive laws, we must determine the state errors and parameter estimation errors as follows:

$$\tilde{\mathbf{x}} = [\tilde{x}_1\ \tilde{x}_2\ \tilde{x}_3\ \tilde{x}_4\ \tilde{x}_5\ \tilde{x}_6]^T = [x_1 - x_d\ x_2\ x_3\ x_4\ x_5 - y_d\ x_6]^T \quad (19)$$

$$\tilde{\mathbf{K}} = [\tilde{K}_1\ \tilde{K}_2\ \tilde{K}_3\ \tilde{K}_4\ \tilde{K}_5\ \tilde{K}_6]^T = [K_1 - \hat{K}_1\ K_2 - \hat{K}_2\ K_3 - \hat{K}_3K_4 - \hat{K}_4\ K_5 - \hat{K}_5\ K_6 - \hat{K}_6]^T. \quad (20)$$

B. Control Laws

The system is feedback linearizable due to the fact that $\mathbf{B}(\mathbf{x}, \mathbf{K})$ is invertible, referring to (18) shown below, provided that $K_i \neq 0$, $\forall i = 1 \sim 6$

$$|\mathbf{B}(\mathbf{x}, \mathbf{K})| = -8K_1K_4^2d_{m1}d_{M1}\begin{vmatrix} K_3 & 2K_1x_6 & 0 \\ K_3x_6 & -2K_1 & \frac{m}{M+m}K_6 \\ -K_3x_6 & 2K_1 & K_6 \end{vmatrix} = 16\frac{M+2m}{M+m}d_{m1}d_{M1}\left(1+x_6^2\right)K_1^2K_3K_4^2K_6. \quad (21)$$

If all the parameters and states are known, then we can choose the control inputs as

$$\mathbf{u} = \mathbf{B}^{-1}(\mathbf{x}, \mathrm{K})\left[-\mathbf{f}(\mathbf{x}, \mathrm{K}) - \mathbf{G_D}\dot{\mathbf{x}} - \mathbf{G_p}\mathbf{x}\right] \quad (22)$$

where $\mathbf{G_p} = \text{diag}(p_i, \ldots, p_6)$ is a position gain $\mathbf{G_D} = \text{diag}(d_i, \ldots, d_6)$ and is a velocity gain. Then, (18) can be in the form

$$\mathbf{D}\ddot{\mathbf{x}} + \mathbf{G_D}\dot{\mathbf{x}} + \mathbf{G_p}\mathbf{x} = 0. \quad (23)$$

By choosing $\mathbf{G_D}, \mathbf{G_p}$ properly, we can make the roots of (23) real and negative. Thus, the control goals can be easily achieved. In fact, the force constants $\mathbf{K}$ are unknown; therefore, the control inputs are chosen by replacing the unknown constants with their estimated values

$$\mathbf{u} = \mathbf{B}^{-1}(\mathbf{x}, \hat{\mathrm{K}})\left[-\mathbf{f}(\mathbf{x}, \hat{\mathrm{K}}) - \mathbf{G_D}\dot{\mathbf{x}} - \mathbf{G_p}\mathbf{x}\right]. \quad (24)$$

In the above derivation, we have used the fact that $\mathbf{f}(\mathbf{x}, \mathbf{K})$ and $\mathbf{B}(\mathbf{x}, \mathbf{K})$ are linear in $\mathbf{K}$ so that we can define the estimation errors $\mathbf{f}(\mathbf{x}, \tilde{\mathbf{K}}) = \mathbf{f}(\mathbf{x}, \mathbf{K}) - \mathbf{f}(\mathbf{x}, \hat{\mathbf{K}})$ and $\mathbf{B}(\mathbf{x}, \tilde{\mathbf{K}}) = \mathbf{B}(\mathbf{x}, \mathbf{K}) - \mathbf{B}(\mathbf{x}, \hat{\mathbf{K}})$. Thus, the closed-loop system after substituting (24) into (18) becomes

$$\begin{aligned} \mathbf{D}\ddot{\mathbf{x}} &= \mathbf{f}(\mathbf{x}, \mathbf{K}) + \mathbf{B}(\mathbf{x}, \mathbf{K})\mathbf{B}^{-1}(\mathbf{x}, \hat{\mathbf{K}}) \left[-\mathbf{f}(\mathbf{x}, \hat{\mathbf{K}}) - \mathbf{G_D}\dot{\mathbf{x}} - \mathbf{G_P}\mathbf{x}\right] \\ &= \mathbf{f}(\mathbf{x}, \mathbf{K}) + \left[\mathbf{B}(\mathbf{x}, \tilde{\mathbf{K}}) + \mathbf{B}(\mathbf{x}, \hat{\mathbf{K}})\right]\mathbf{B}^{-1}(\mathbf{x}, \hat{\mathbf{K}}) \left[-\mathbf{f}(\mathbf{x}, \hat{\mathbf{K}}) - \mathbf{G_D}\dot{\mathbf{x}} - \mathbf{G_P}\mathbf{x}\right] \\ &= \mathbf{f}(\mathbf{x}, \mathbf{K}) - \mathbf{f}(\mathbf{x}, \hat{\mathbf{K}}) - \mathbf{G_D}\dot{\mathbf{x}} - \mathbf{G_P}\mathbf{x} \\ &\quad + \mathbf{B}(\mathbf{x}, \tilde{\mathbf{K}})\mathbf{B}^{-1}(\mathbf{x}, \hat{\mathbf{K}})\left[-\mathbf{f}(\mathbf{x}, \hat{\mathbf{K}}) - \mathbf{G_D}\dot{\mathbf{x}} - \mathbf{GPx}\right] \\ &= \mathbf{f}(\mathbf{x}, \tilde{\mathbf{K}}) + \mathbf{B}(\mathbf{x}, \tilde{\mathbf{K}})\mathbf{u} - \mathbf{G_D}\dot{\mathbf{x}} - \mathbf{G_P}\mathbf{x}. \end{aligned} \quad (25)$$

We next define

$$\mathbf{S} = \dot{\mathbf{x}} + \Lambda_1\mathbf{x} \quad (26)$$

where $\Lambda_1 = \text{diag}(\lambda_1, \lambda_2, \ldots, \lambda_6)$ is chosen to be positive definite and $\mathbf{S} = [s_1\ s_2 \cdots\ s_6]^T$. Then, we choose $\Lambda_2 = \text{diag}(\lambda_1', \lambda_2', \ldots, \lambda_6')$ to be positive definite, and rederive the closed-loop dynamics due to the control input (24) in terms of $\mathbf{S}$ by differentiating (26) and incorporating (25) as follows:

$$\mathbf{D}\dot{\mathbf{S}} = \mathbf{D}\ddot{\mathbf{x}} + \mathbf{D}\Lambda_1\dot{\mathbf{x}} = \mathbf{f}(\mathbf{x}, \tilde{\mathbf{K}}) + \mathbf{B}(\mathbf{x}, \tilde{\mathbf{K}})\mathbf{u} - \mathbf{G_D}\dot{\mathbf{x}} - \mathbf{G_P}\mathbf{x} + \mathbf{D}\Lambda_1\dot{\mathbf{x}}$$

or

$$\mathbf{D}\left(\dot{\mathbf{S}} + (\mathbf{D}^{-1}\mathbf{G_D} - \Lambda_1)\dot{\mathbf{x}} + \mathbf{D}^{-1}\mathbf{G_P}\mathbf{x}\right) \triangleq \mathbf{D}(\dot{\mathbf{S}} + \Lambda_2\mathbf{S}) = \mathbf{f}(\mathbf{x}, \tilde{\mathbf{K}}) + \mathbf{B}(\mathbf{x}, \tilde{\mathbf{K}})\mathbf{u} \quad (27)$$

provided that $\mathbf{G_p} = \mathbf{D}\Lambda_2\Lambda_1$ and $\mathbf{G_D} = \mathbf{D}\Lambda_2 + \mathbf{D}\Lambda_1$.

C. Adaptive Laws

Due to the estimates used in the control inputs, some adaptive laws must be adopted. The adaptive laws are designed follows:

$$\begin{aligned}
\dot{\hat{K}}_1 &= g_1 \{2(s_1u_2x_6 - s_2u_2 - d_{m1}s_3u_3 - s_4x_6u_2 + s_5u_2) \\
&\quad + s_6[2(x_1 - x_4)u_2 + 2d_{m1}u_3 \\
&\quad + (x_3 - X_6)((d_{m2} + d_{m3})u_2 + (d_{m3} - d_{m2})u_3)]\} \\
\dot{\hat{K}}_2 &= 4g_2\{s_2(x_2 - x_1x_6) + d_{m1}^2 s_3(x_3 - x_6) \\
&\quad - s_5(x_2 - x_1x_6) - s_6[x_1(x_2 - x_1x_3) \\
&\quad + d_{m1}^2(x_3 - x_6)]\} \\
\dot{\hat{K}}_3 &= g_3[s_1u_1 + s_2x_6u_1 - s_4u_1 - s_5x_6u_1] \\
\dot{\hat{K}}_4 &= -2g_4[s_4u_4 + d_{M1}s_6u_6] \\
\dot{\hat{K}}_5 &= 4g_5[x_4s_4 + d_{M1}^2 s_6x_6] \\
\dot{\hat{K}}_6 &= g_6\left[\frac{m}{M+m}s_2u_4 + s_5u_5\right]
\end{aligned} \tag{28}$$

where $g_i > 0, \forall i = 1 \sim 6$. Then, combining the adaptive laws and the control laws, the states and their velocities can be shown to be asymptotically stable, as we will demonstrate in the next section.

Remark: It should be noted that, to guarantee that $\mathbf{B}(\mathbf{x}, \hat{\mathbf{K}})$ is invertible so that the control law (24) is well-defined, some parameter projection laws [17] need to be incorporated into the adaptive laws in (28). We assume that $|K_i| \geq \eta_i > 0$, for $i = 1 \sim 6$. Let us denote the nominal vector field by $\tau = [\tau_1, \tau_2, \ldots, \tau_6]^T$ and choose $\varepsilon \in (0, \eta_i)$. The projection operator is given by (29) shown at the bottom of the page.

D. Stability Analysis

In order to prove the stability of (24) using the control law in (23) and the adaptive law in (28), we employ the Lyapunov function candidate V as follows:

$$V = \frac{1}{2}[\widetilde{\mathbf{K}}^T\mathbf{G}^{-1}\widetilde{\mathbf{K}} + \mathbf{S}^T\mathbf{D}\mathbf{S}] \tag{30}$$

where $\mathbf{G} = \mathrm{diag}(g_1, \ldots, g_6)$, whose time derivative can be evaluated as

$$\begin{aligned}
\dot{V} &= \widetilde{\mathbf{K}}^T\mathbf{G}^{-1}\dot{\widetilde{\mathbf{K}}} + \mathbf{S}^T\mathbf{D}\dot{\mathbf{S}} \\
&= \widetilde{\mathbf{K}}^T\mathbf{G}^{-1}\dot{\widetilde{\mathbf{K}}} + \mathbf{S}^T\left[-\mathbf{D}\Lambda_2\mathbf{S} + \mathbf{f}(\mathbf{x}, \widetilde{\mathbf{K}}) + \mathbf{B}(\mathbf{x}, \widetilde{\mathbf{K}})\mathbf{u}\right] \\
&\quad - \mathbf{S}^T\mathbf{D}\Lambda_2\mathbf{S} + \widetilde{\mathbf{K}}^T G^{-1}\widetilde{\mathbf{K}} + \mathbf{S}^T\left[\mathbf{f}(\mathbf{x}, \widetilde{\mathbf{K}}) + \mathbf{B}(\mathbf{x}, \widetilde{\mathbf{K}})\mathbf{u}\right] \\
&= \mathbf{S}^T\mathbf{D}\Lambda_2\mathbf{S} \leq 0.
\end{aligned} \tag{31}$$

From (30) and (31), it can be seen that V is a suitable Lyapunov function. By using the Lyapunov stability theory, we can conclude that $\widetilde{\mathbf{K}}$ and $\mathbf{S}$ are all bounded, that $s_i \in L_2$ and, in turn, that $\dot{s}_i \in L_\infty$ by referring back to (24). Thus, by using Barbalat's Lemma [18], we can conclude have that s_i is asymptotically stable, which implies that $\widetilde{x}_i, \dot{\widetilde{x}}_i$ go to zero as time goes to infinity. As a result, the control objectives described above are achieved; hence, Subsystems I and II are kept at the center of the upper guiding tracks and ground guiding tracks, respectively.

TABLE I
SYSTEM HARDWARE PARAMETERS

		Sub-system I	Sub-system II
Mass		0.5Kg	3Kg
Moment of inertia		0.04Kg.m^2	0.5 Kg.m^2
Stabilizing force constant		-12.6 N/A	-63.7N/A
Destabilizing force constant		243N/m	1215N/m
VCM force constant		30N/A	80N/A
Stabilizer	coil diameter	0.4mm	0.5mm
	number of wires	200	260
	track size	10×12×150mm	20×20×400mm
	NdFeB size	8×20×30mm	10×25×100mm
Levitator	coil diameter	0.3mm	0.5mm
	number of wires	100	160
	track size	20×10×200mm	20×20×400mm
	NdFeB size	8×2×200mm	10×2×400mm
VCM	coil diameter	0.4mm	0.5mm
	number of wires	200	300
	aircore size	30×20×80mm	40×20×120mm
	total size	50×40×80mm	60×40×120mm

d_{m1}=64mm, d_{m2}=40mm, d_{m3}=62mm,d_{M1}=90mm, d_{M2}=75mm, d_{M3}=133mm

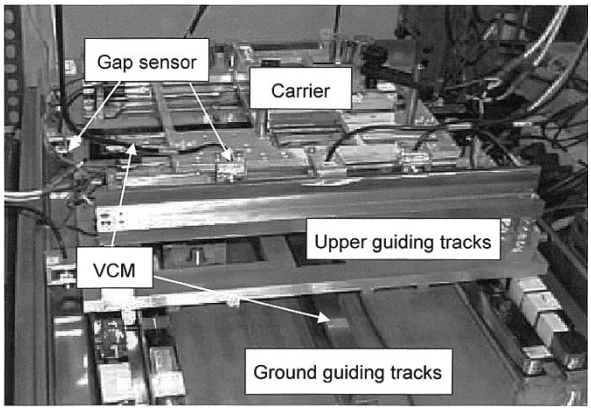

Fig. 9. Photograph of the physical setup of the dual-axis Maglev system.

IV. EXPERIMENTAL RESULTS

The experimental hardware, including the main body, sensor system, driver system and controller hardware, will be described here. The parameters of the experimental setup are listed in Table I, and Fig. 9 shows photographs of the dual-axis Maglev system physical set-up. A number of experimental results, including the transient and the steady-state responses in different

$$\dot{\hat{K}}_i = \tau_i \begin{cases} 1, & \hat{K}_i \mathrm{sgn} K_i > \eta_i \text{ or } \tau_i \mathrm{sgn} K_i \geq 0 \\ \max\left\{0, \frac{\varepsilon_i - \eta_i + \hat{K}_i \mathrm{sgn} K_i}{\varepsilon_i}\right\}, & \hat{K}_i \mathrm{sgn} K_i \leq \eta_i \text{ and } \tau_i \mathrm{sgn} K_i < 0. \end{cases} \tag{29}$$

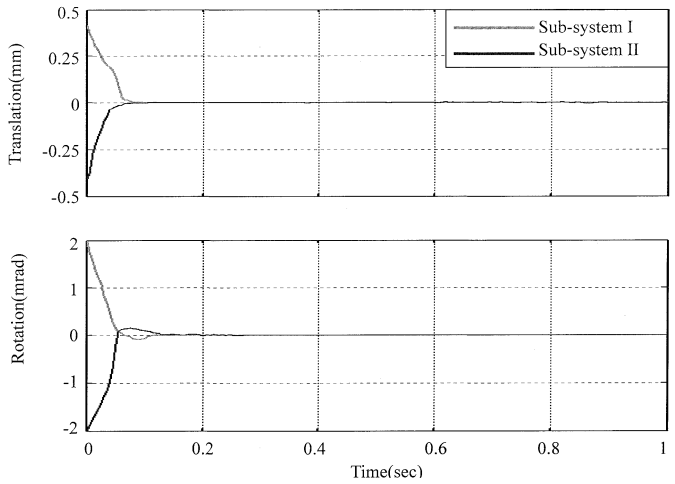

Fig. 10. Transient response of the adaptive controller.

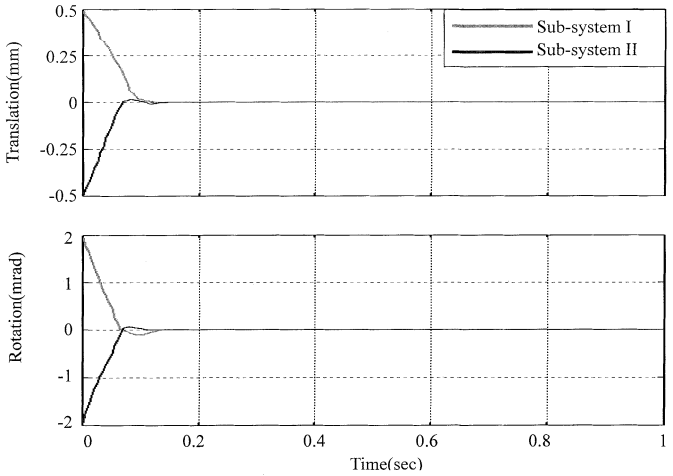

Fig. 11. Transient response of the adaptive controller when a load of 100g was employed.

situations, will also be provided in this section to demonstrate the performance of this system with the controller presented in Section III. Based on these results, we will discuss some important aspects of future research.

A. Hardware Implementation

This sensor system is divided into lateral sensor subsystems, which provides two- translational and two-rotational displacement data for the controller. Two identical gap sensor pairs are mounted on Subsystems I and II, and their physical locations are shown in Fig. 2. The model number of the gap sensor is AS-440-02, and it is manufactured by the KEYENCE Corporation, Japan. The gap sensor has a 0∼2 mm range of measurement (ROM) with a resolution of 0.1% of ROM and the bandwidth of the sensor is 3.3 kHz.

The function of drivers in our system is to provide sufficient current to the stabilizing and levitating coils. Because the current instead of the voltage is used as the control input, the current drivers must have high enough bandwidth. The drivers we currently used are EM-19 linear amplifiers manufactured by Kollmorgen Inc. in the U.S. They are linear drivers designed to be servo drivers for DC motors.

The current microcomputer we use is an IBM PC with a Pentium microprocessor inside. The clock rate is 233 MHz, which allows us to accomplish real-time control implementation. The ADC we use is a 12-bit high resolution data acquisition adapter, and the DAC altogether has six converting channels with 12-bit resolution each. Based on the experiential results, we conclude that a sampling time between 0.1 and 0.05 ms leads to better behavior of this system.

B. System Performance

Before we investigate the transient responses of the closed-loop system, some specifications should be discussed. First, the full X direction translational range was limited to $\pm 1\ mm$, whereas the Z-axis full rotational range was ± 0.2 radian. On the other hand, we compared the performance of the two cases, respectively, with no load and with a 100 g load. The symbols x_1 and x_3 represent the translational and rotational displacements of Subsystem I whereas x_4 and x_6 represent the translational and rotational displacements of Subsystem II. The control parameters for the adaptive controller were set as $\Lambda_1 = \mathrm{diag}(1,5,1,3,10,3)$ and $\mathbf{G_P} = \mathrm{diag}(300\,500\,200\,600\,800\,550)$, $\mathbf{G_D} = \mathrm{diag}(25,35,20,60,75,50)$.

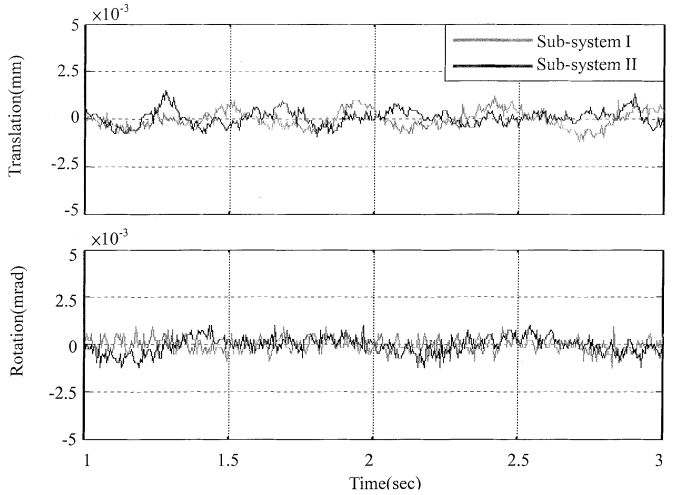

Fig. 12. Steady-state response of the adaptive controller.

1) Transient Response: To verify that the adaptive controller framework could ensure that the dual-axis Maglev system could achieve stable regulation as opposed to its original unstable nonlinear nature, Fig. 10 shows the transient response of the adaptive controller with respect to the worse case (maximal displacement). We can observe that the rising time for Subsystem I was 0.08 s, and that the settling time was 0.11 s, whereas the rising time for Subsystem II was 0.08 s, and the settling time was 0.1 s. The magnitude of rotational overshoot on that Subsystem I was 0.1 mrad, and that on Subsystem II was 0.05 mrad. Fig. 11 shows the performance when Subsystem I was subjected to a load of 100 g. This is exactly the salient feature of the adaptive controller, which can adjust its controller on-line so as to adapt to changes in the environment and ensure the best possible system performance.

2) Steady-State Response: The positioning precision of our system is determined by the steady-state response of Subsystem I. Figs. 12 and 13 show the system responses around

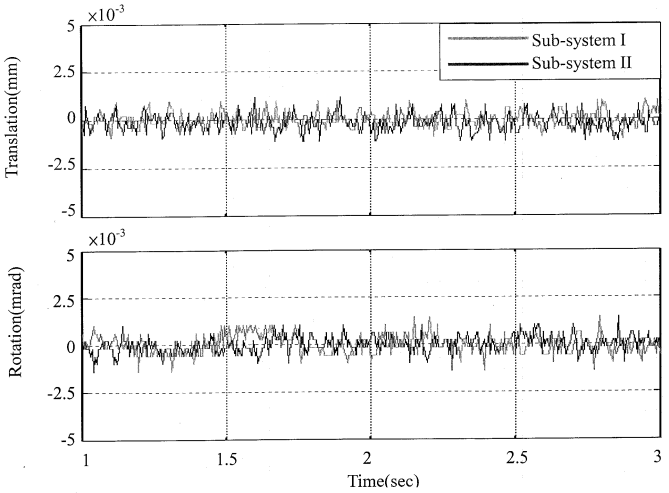

Fig. 13. Steady-state response of the adaptive controller when a load of 100g was employed.

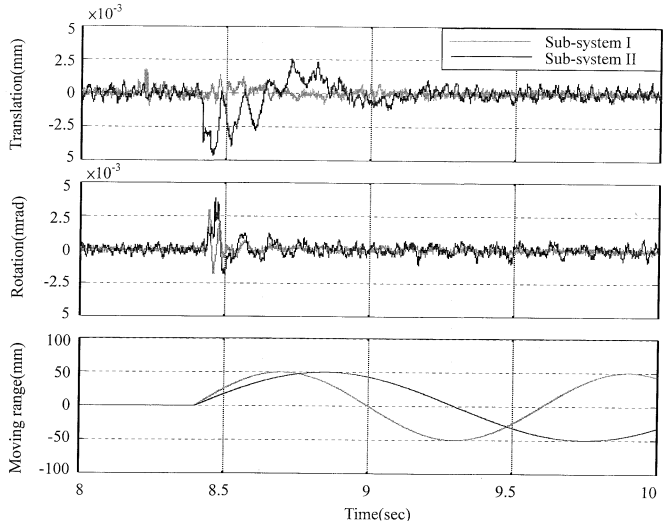

Fig. 14. Response of the adaptive controller with a reference trajectory.

the operating points for an no load and a 100 g load, subject to the largest translation displacement. These results show that the adaptive controller is superior in terms of its ability to regulate performance, even when Subsystem I load varies.

3) Moving Along the Position Axis in a Harmonic Motion Test: Fig. 14 shows the experimental results obtained when the desired Subsystem I position was $x_d = 0.05\sin(30\mathrm{t})$ m and that of Subsystems II was $y_d = 0.05\sin(20\mathrm{t})$ m. The initial state conditions were assigned randomly. When the guiding system was stable, its stability was slightly affected only at the instant when the modified VCM started to drive the stage in the Y direction; however, the guiding precision was not affected. In our VCM structure, the above means that a propulsive force is mainly produced in X and Y directions. On the other hand, our guiding controller can also effectively reject this disturbance via the proposed adaptive controller.

C. Discussion

Besides manufacturing and alignment imperfections, vibrations from the interior of the building or from the mechanism

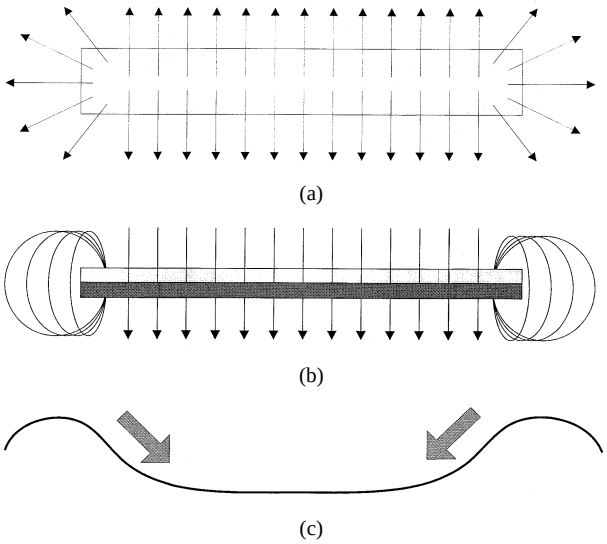

Fig. 15. Edge effect. (a) Top view of the magnetic flux distribution. (b) Side view of the magnetic flux distribution. (c) Potential enery curve.

may affect system responses. Other important conclusions are drawn in the following.

1) Edge Effect: In modeling, we always assume that the length of a guiding track is infinitely long so that we can simplify the derivation of the electromagnetic equations and, in turn, further makes our system easier to understand. However, the length of the track employed here is only 40 cm. The edge effect, therefore, does appear in our application.

Fig. 15(a) and (b) shows two different views of the magnetic flux distribution of an oblong magnet. The flux density around the two edges is higher than that of the other area. Between the two edges, the magnetic field is rather uniform, which implies the existence of small magnetic field gradients; hence the magnetic field complies with our assumption. On the other hand, the larger gradients near the two edges are far from the assumed ideal case.

Indeed, the nonuniform magnetic field in the VCM moving direction will impose a constraint force which will invalidate our system requirement. For a repulsive Maglev, the direction of the constraint force should be clear from Fig. 15(c), which depicts the curve of the potential energy. From the viewpoints of energy conservation and thermodynamics, the carrier will slide back and forth by repeatedly converting potential energy to kinetic energy vice versa until all the energy consumed by some resisting force becomes heat. In other words, the carrier will eventually stop moving at the midpoint of the track due to the existence of damping forces.

2) Damping Forces: As for the damping forces, there are three sources in general. They are air damping, electromagnetic force (emf), and eddy current losses resulting from the dynamic magnetic field.

First, it is difficult to reduce the air damping to the point where it is negligible unless that we can provide a vacuum environment for operation. Second, the emf effect is relatively insignificant since all the coils in our system are current-controlled. Therefore, the last and also most important factor is the eddy current losses, as will be explained below.

The currents circulating in metallic materials subject to an emf induced by a varying magnetic field give rise to eddy current losses. Although the permeability of the material we used in the tracks, aluminum, is pretty small, its conductivity inevitably leads to eddy current losses. The kinetic energy, therefore, dissipates gradually due to these energy losses until the system reaches its minimum potential energy.

V. Conclusion

In this paper, a larger moving range dual-axis Maglev system has been presented. A repulsive Maglev system with four active guiding tracks was adopted here. The system was treated as a multi-input multi-output system, and an adaptive controller was designed. By means of experimental results, the system's feasibility and effectiveness have been clearly demonstrated. Excellent performance in terms of regulation of the guiding-axis and tracking for the positioning-axis has been achieved. These results can aid future design work on noncontact magnetic positioning systems.

References

[1] R. L. Hollis, S. E. Salcudean, and A. P. Allan, "A six-degree-of-freedom magnetically levitated variable compliance fine-motion wrist: Design, modeling, and congrol," *IEEE Trans Robot. Automat.*, vol. 7, pp. 320–332, June 1991.

[2] P. K. Sinha, *Electromagnetic Suspension: Dynamics and Control*. Stevenage, U.K.: Peregrinus, 1987.

[3] B. V. Jayawant, *Electromagnetic Levitation and Suspension Techniques*. London, U.K.: E. J. Arnold, 1981.

[4] H. Bleuler, "A suvey of magnetic levitation and magnetic bearing types," *JSME Int. J., Vibrat., Control Eng., Eng. Ind.*, ser. 3, vol. 35, no. 3, pp. 563–568, Sept. 1992.

[5] L.-C. Lin and T.-B. Chau, "Feedback linearization and fuzzy control for conical magnetic bearings," *IEEE Trans. Contr. Syst. Technol.*, vol. 5, pp. 417–426, July 1997.

[6] K. Park *et al.*, "Magnetic levitated high precision positioning system based on antagonistic mechanism," *IEEE Trans. Magn.*, vol. 32, pp. 208–219, Jan. 1996.

[7] S.-R. Oh, R. L. Hollis, and S. E. Salcudean, "Precision assembly with a magnetically levitated wrist," in *Proc. IEEE Int. Conf. Robotics and Automation*, Atlanta, GA, 1993, pp. 127–134.

[8] E. Nakamoto, Q.-M. Chen, and H. Takenuchi, "Electromagnetic and structure coupled finite element analysis of active control in an anti-vibration device," *IEEE Trans. Magn.*, vol. 33, pp. 1666–1669, Mar. 1997.

[9] F. N. Koumboulis, "Static controllers for magnetic suspension and balance systems," *Proc. Inst. Elect. Eng. Control Theory and Applications*, vol. 143, no. 4, pp. 338–348, July 1996.

[10] D. L. Trumper, S. M. Olson, and P. K. Subrahmanyan, "Modeling and vector control of a planar magnetic levitator," *IEEE Trans. Ind. Applicat.*, vol. 34, pp. 1254–1262, Nov./Dec. 1998.

[11] K. H. Park, "Wafer distribution system for a clean room using a novel magnetic suspension technique," *IEEE/ASME Trans. Mechatron.*, vol. 3, pp. 73–78, Mar. 1998.

[12] I. Y. Wang and B. V. Ilene, "A new repulsive magnetic levitation approach using permanent magnets and air-core electromagnets," *IEEE Trans. Magn.*, vol. 30, pp. 1422–1432, July 1994.

[13] M. Y. Chen, K. N. Wu, and L. C. Fu, "Adaptive control and experiment of a Maglev guiding system for wafer transportation," in *Proc. I.F.A.C. Workshop Motion Control Conf.*, Grenoble, France, 1998, pp. 263–268.

[14] ——, "Design, implementation and self tuning adaptive control of a Maglev guiding system," *Mechatron.*, pp. 215–237, 2000.

[15] M. Y. Chen, M. J. Wang, and L. C. Fu, "Modeling and controller design of a Maglev guiding system for application in precision positioning," in *Proc. Amer. Control Conf.*, San Diego, CA, 1999, pp. 3072–3076.

[16] ——, "Dual-axis Maglev guiding system modeling and controller design for wafer transportation," in *Proc. Control and Decision Conf.*, Phoenix, AZ, 1999, pp. 2623–2628.

[17] M. Krstic, I. Kanellakopoulos, and P. Kokotovic, *Nonlinear and Adaptive Control Design*. New York: Wiley Interscience, 1995.

[18] J.-J. E. Slotine and W. Li, *Applied Nonlinear Control*. Englewood Cliffs, NJ: Prentice-Hall, 1990.

Mei-Yung Chen (S'99) was born in Maju, Taiwan, R.O.C., in 1966. He received the B.S. degree from TamKang University, Taipei, Taiwan, R.O.C., in 1992, the M.S. degree from Chung Yuan Christian University, Chung-Li, Taiwan, R.O.C., in 1994, and is currently working toward the Ph.D. degree in the Department of Electrical Engineering, National Taiwan University, Taipei, R.O.C.

Currently, he is a Teaching Assistant in the Automatic Control Laboratory, Department of Electrical Engineering, National Taiwan University. His areas of research interest include magnetic levitation technology, positioning and tracking, mechatronics, and control theory and applications.

Mr. Chen is a Member of the Chinese Automatic Control Society. He received the Best Student Paper Award from the Chinese Automatic Control Society in 2001.

Ming-Jyh Wang was born in Tainan, Taiwan, R.O.C., in 1974. He received the B.S. degree from the Department of Control Engineering, National Chiao-Tung University, Hsin-Chu, Taiwan, R.O.C. and the M.S. degree from the Department of Electrical Engineering, National Taiwan University, Taipei, Taiwan, R.O.C., in 1996 and 1998, respectively.

Since 1998, he has been with Chung-Shan Institute of Science and Technology, Chung-Li, Taiwan, R.O.C., where he has been involved in the design of airborne computer and multimedia application. His research interests include system integration, adaptive control and circuit design.

Li-Chen Fu (S'85–M'88–SM'91) was born in Taipei, Taiwan, R.O.C., in 1959. He received the B.S. degree from National Taiwan University, Taipei, in 1981 and the M.S. and Ph.D. degrees from the University of California, Berkeley, in 1985 and 1987, respectively.

Since 1987, he has been a member of the faculty, and is currently a Professor in both the Department of Electrical Engineering and Department of Computer Science and Information Engineering, National Taiwan University, where he also served as the Deputy Director of the Tjing Ling Industrial Research Institute, from 1999 to 2001. His research interests include robotics, FMS scheduling, shop floor control, home automation, visual detection and tracking, E-commerce, and control theory and applications.

Dr. Fu is a Senior Member of the IEEE Robotics and Automation and IEEE Automatic Control Societies. He is also a Member of the Boards of the Chinese Automatic Control Society and Chinese Institute of Automation Engineers. From 1996 to 1998 and in 2000, he was appointed as a Member of the IEEE Robotics and Automation Society AdCom and will serve as the Program Chair of the 2003 IEEE International Conference on Robotics and Automation. He received the Excellent Research Award for 1990 to 1993 and Outstanding Research Awards in 1995, 1998, and 2000 from the National Science Council, R.O.C. He also received the Outstanding Youth Medal in 1991, the Outstanding Engineering Professor Award in 1995, and the Best Teaching Award in 1994 from the Ministry of Education, the Ten Outstanding Young Persons Award in 1999 from the R.O.C., the Outstanding Control Engineering Award from the Chinese Automatic Control Society in 2000, and the Lee Kuo-Ding Medal from the Chinese Institute of Information and Computing Machinery, in 2000. He has been the Editor of the *Journal of Control and Systems Technology* and an Associate Editor of the prestigious control journal, *Automatica*. In 1999, he became the Editor-in-Chief of a new control journal, *Asian Journal of Control*